

The Atmospheric Dynamics of Intraseasonal Length-of-Day Fluctuations during the Austral Winter

STEVEN B. FELDSTEIN

Earth System Science Center, The Pennsylvania State University, University Park, Pennsylvania

(Manuscript received 24 April 1998, in final form 29 October 1998)

ABSTRACT

The atmospheric dynamical processes associated with intraseasonal length-of-day (LOD) variability during the austral winter are examined with National Centers for Environmental Prediction–National Center for Atmospheric Research reanalysis and outgoing longwave radiation (OLR) data. The method adopted is to regress the relevant fields against the LOD tendency. All quantities in this study are bandpassed through a 30–70-day filter.

The findings from an analysis of the OLR and 200-mb eddy streamfunction fields are consistent with the idea that large intraseasonal LOD fluctuations coincide with an active Madden–Julian oscillation (MJO). Further analysis suggests that the eddy response to the MJO heating drives both an anomalous meridional circulation that excites the anomalous global friction torque, and an eddy field that has the appropriate location relative to the topography for generating the anomalous global mountain torque. These results were obtained by calculating regressions of the anomalous eddy angular momentum flux convergence, mass streamfunction, surface stress, and surface pressure fields, and each term in the lowest sigma level relative angular momentum budget.

The anomalous global friction and mountain torques are found to be of similar magnitude, with the former leading the latter by eight days. The largest contribution toward the anomalous global friction (mountain) torque comes from Australia and the surrounding ocean (the Andes).

1. Introduction

Intraseasonal length-of-day (LOD) and atmospheric angular momentum (AAM) fluctuations have been a subject of increasing interest during the past 15 years. Interest in this subject has in large part been motivated by the highly accurate space-based geodetic measurements of the LOD and the increasingly accurate global atmospheric observations (Rosen 1993). Both sets of measurements revealed large contemporaneous correlations between globally integrated AAM (GAAM) and LOD on timescales less than 10 yr (e.g., Hide et al. 1980; Langley et al. 1981; Rosen and Salstein 1983; Hide and Dickey 1991). Such behavior, together with the observed amplitude of the LOD and GAAM changes, indicates that the exchange of angular momentum between the atmosphere and solid earth does not involve significant changes in the oceanic angular momentum. Furthermore, many studies have found statistically significant intraseasonal fluctuations in both LOD and GAAM with a period of approximately 50 days (e.g., Langley et al. 1981; Rosen and Salstein 1983; Lau et

al. 1989; Dickey et al. 1991; Magana 1993), a period that overlaps with the tropical Madden–Julian oscillation (MJO; Madden and Julian 1971, 1972). More recently, several studies have verified that the large intraseasonal LOD and GAAM fluctuations do indeed overlap with periods of active MJOs (e.g., Weickmann et al. 1992; Magana 1993; Weickmann and Sardeshmukh 1994; Hendon 1995).

Most of the earliest LOD–AAM studies emphasized the spatial and temporal characteristics of the AAM field itself (e.g., Anderson and Rosen 1983; Rosen and Salstein 1983). However, within the past several years, researchers have broadened their investigation to include an examination of the quantities that drive the LOD–AAM fluctuations, that is, the friction and mountain torques, in addition to the atmospheric variables that are suspected of generating these torques. This approach includes both observational studies (e.g., Kang and Lau 1990; Weickmann et al. 1992; Ponte and Rosen 1993; Weickmann and Sardeshmukh 1994; Hendon 1995; Madden and Speth 1995; Weickmann et al. 1997) and also those with idealized numerical models (Itoh 1994) and GCMs (Feldstein and Lee 1995). However, most of these studies either use data that span the entire year, or restrict examination to the boreal winter. As a result, there has been little attention focused on the LOD–AAM fluctuations of the austral winter.

Corresponding author address: Dr. Steven B. Feldstein, Earth System Science Center, The Pennsylvania State University, 248 Deike Building, University Park, PA 16802.
E-mail: sbf@essc.psu.edu

Two studies that do examine austral winter intraseasonal GAAM fluctuations are Kang and Lau (1990) and Weickmann et al. (1992). They find that the intraseasonal GAAM fluctuations are associated with friction torques in the central tropical Pacific Ocean. Weickmann et al. (1992) also estimate the globally integrated friction torque and find a temporal in-phase relationship with the GAAM tendency. These results indicate that unless the globally integrated mountain torque is in phase with globally integrated friction torque, the globally integrated mountain torque must be relatively small during large austral winter intraseasonal LOD–GAAM fluctuations. However, as observed values of the surface stress were not readily available at the time of these studies, the authors resorted to inferring the surface stress field, and hence the friction torque, from the observed 850-mb wind field. More recently, these estimates of the friction torque have come into question, as Itoh (1994) presented results showing that the use of the 850-mb winds for estimating the friction torque leads to a large overestimation within the Tropics.

The above studies clearly reveal that many of the basic features of austral winter intraseasonal LOD–GAAM fluctuations have yet to be documented. Noting the above problem of estimating the tropical friction torque with the 850-mb winds, important issues that need to be addressed for the austral winter include 1) the relative role of the friction and mountain torques and 2) the geographical locations that account for the largest contribution to these torques. A more interesting challenge, however, is to explain the underlying atmospheric dynamical processes that determine these torques. Although more definitive statements on these dynamical processes require the use of simplified models, much can be learned about these dynamical processes with an appropriate selection of diagnostic techniques applied to observational data. In this study, we follow the latter approach to address issues such as whether convectively driven Rossby waves excite the torques and whether the anomalous friction torque is forced by an eddy-driven meridional circulation. For this purpose, the National Centers for Environmental Prediction–National Center for Atmospheric Research (NCEP–NCAR) reanalysis dataset is used. One particular advantage to this dataset is that the daily surface stress field is provided.

The data and methodology are presented in section 2. This is followed in section 3 by a detailed documentation of the friction and mountain torques. Section 4 presents the results of a diagnostic analysis of the outgoing longwave radiation (OLR), eddy streamfunction, mass streamfunction, and surface pressure. The conclusions are presented in section 5.

2. Data and methodology

Most fields to be presented in this study are derived from daily (0000 UTC) NCEP–NCAR reanalysis data

extending from 1 January 1979 to 31 December 1995. This includes the friction and mountain torques, eddy AAM flux convergence, 200-mb streamfunction, surface pressure, and mass streamfunction. Additional quantities utilized are the LOD timeseries, which was kindly provided by P. Nelson of Atmospheric and Environmental Research, Inc.; and OLR, which is produced by the National Oceanic and Atmospheric Administration. The latter quantity is used as a proxy measurement for convection within the Tropics. As stated in the previous section, this investigation of intraseasonal LOD–GAAM variability is being applied to the austral winter, which we define as the months of May through September.

The zonally and vertically integrally absolute angular momentum $M(\theta, t)$ can be defined in sigma coordinates as

$$M(\theta, t) = \frac{a^2}{g} \int_0^{2\pi} \int_0^1 p_s (u + \Omega a \cos\theta) \cos^2\theta \, d\sigma \, d\lambda, \quad (1)$$

where u and p_s denote the zonal wind and surface pressure, respectively; σ , λ , and θ the vertical, longitudinal, and latitudinal coordinates; t time; a the earth's radius; Ω the earth's angular velocity; and g the gravitational acceleration. The corresponding equation for the conservation of $M(\theta, t)$ can be written as

$$\frac{\partial M}{\partial t} = -\frac{1}{a \cos\theta} \int_0^{2\pi} \int_0^1 \frac{\partial}{\partial \theta} \left(\frac{p_s \mu v \cos\theta}{g} \right) a \cos\theta \, d\sigma \, d\lambda + T_F + T_M + T_G, \quad (2)$$

where $\mu = (u + \Omega a \cos\theta)a \cos\theta$, v is the meridional wind, T_F the friction torque, T_M the mountain torque, and T_G the gravity wave drag torque, which is included in (2) for completeness. (Note, however, that T_G associated with the intraseasonal LOD–GAAM fluctuations is found to be substantially smaller than the other torques, so we will not consider it further in this study.) This equation relates the absolute angular momentum tendency to the absolute angular momentum flux convergence and the sum of the three torques. The friction and mountain torques can be expressed as

$$T_M = -a^2 \cos^2\theta \int_0^{2\pi} p_s \frac{\partial h}{\partial x} \, d\lambda; \\ T_F = a^2 \cos^2\theta \int_0^{2\pi} (\tau_\lambda)_{\sigma=1} \, d\lambda, \quad (3)$$

where h is the topographic height, x is the zonal length coordinate, and the sign of the surface stress $(\tau_\lambda)_{\sigma=1}$ is defined to be positive when there is a transfer of angular momentum from the solid earth to the atmosphere. The calculations of these torques are straightforward, as the p_s , h , and $(\tau_\lambda)_{\sigma=1}$ fields are included within the NCEP–NCAR reanalysis dataset. A straightforward latitudinal integration of (2) yields

$$\frac{\partial(\text{GAAM})}{\partial t} = \int_{-\pi/2}^{\pi/2} (T_F + T_M) d\theta. \quad (4)$$

The relationship between the LOD tendency and the torques can then be easily determined with the following relationship: $\delta(\text{LOD}) = 1.68 \times 10^{-29} \delta(\text{GAAM})$ (Rosen and Salstein 1983). The units for GAAM are $\text{kg m}^2 \text{s}^{-1}$ and for LOD, s.

As discussed above, we will also analyze the eddy AAM flux convergence and the mass streamfunction. The eddy AAM flux is defined as $[u^*(p, v)^*]$, where the square brackets denote a zonal mean, and the asterisk a deviation from the zonal mean. The mass streamfunction is obtained from the zonally averaged v by vertically integrating the zonally averaged continuity equation downward from the reanalysis model's top sigma level [this technique is described in Peixoto and Oort (1992)].

With the exception of the mountain torque and OLR, all other quantities are generated from data at rhomboidal-30 horizontal resolution. As the mountain torque is found to exhibit some sensitivity to the horizontal resolution, we have retained the reanalysis model's original triangular-62 horizontal resolution for both the surface pressure and the topographic height fields. The reduction in resolution from triangular 62 to rhomboidal 30 for the other quantities was done to save computer storage. For the zonal mean quantities examined in this study, such resolution changes are expected to be inconsequential. Various tests with limited amounts of data verify this to be the case. The OLR has a resolution of 2.5° longitude by 2.5° latitude. With regard to the vertical resolution, all 28 of the reanalysis model's sigma levels are used for calculating $M(\theta, t)$ and the absolute angular momentum flux convergence. These levels range from $\sigma = 0.995$ to $\sigma = 0.0027$.

All quantities to be presented in this study are generated by first applying a 30–70-day bandpass Fourier filter followed by a linear regression against the 30–70-day bandpass LOD tendency. A 30–70-day filter is selected in order to encompass the periods associated with the MJO. [Not surprisingly, given the large correlation between the LOD and GAAM time series, essentially identical results to those presented in this study are obtained if the regression is performed against the 30–70-day bandpass GAAM tendency. For this set of calculations, the AAM was determined following the procedure in Feldstein (1998).] In the regression equation, the amplitude of the LOD tendency anomaly is always specified as one standard deviation.

Statistical significance is determined from the cross-correlation fields, with the number of degrees of freedom (NDOF) being estimated with the procedure of Davis (1976), that is,

$$\text{NDOF} = N\delta t/\tau, \quad (5)$$

$$\tau = \sum_k C_x(k\delta t)C_y(k\delta t)\delta t, \quad (6)$$

where N is the number of days in the time series; δt is

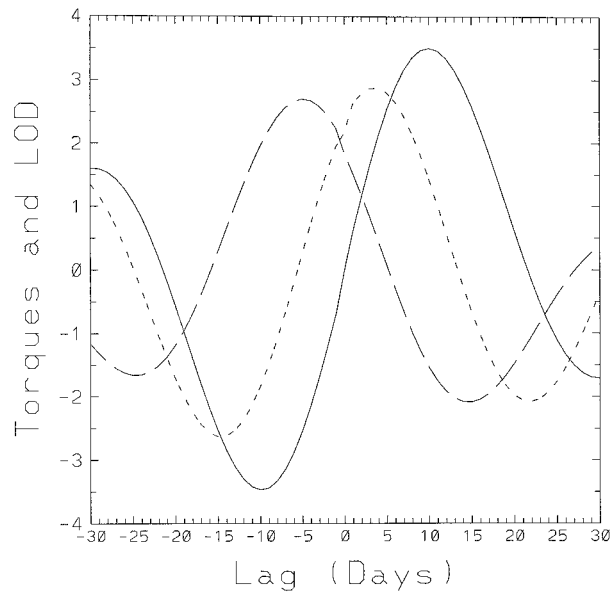


FIG. 1. The anomalous global friction torque (long dashed line), anomalous global mountain torque (short dashed line), and the anomalous LOD (solid line) regressed against the LOD tendency. The torques (LOD) are divided (multiplied) by $1.0 \times 10^{18} \text{ kg m}^2 \text{ s}^{-2}$ (50 ms).

the time interval between adjacent values, that is, one day; and C_x and C_y are the autocorrelations of the LOD tendency and the regressed field, respectively. For most fields and at most latitudes, it is found that NDOF is well in excess of 200.

3. Documentation of the torques

We first examine the temporal evolution of the anomalous global friction and mountain torques and the anomalous LOD, by regressing these quantities against the LOD tendency (Fig. 1). The key features seen are that the maximum values of the two torques are about equal and that the anomalous friction torque leads the anomalous mountain torque by approximately eight days. A similar phase lag is found in most studies of intraseasonal LOD–GAAM variability, both when data from the entire year are used (Hendon 1995) and when the data are limited to the boreal winter (Weickmann and Sardeshmukh 1994; Madden and Speth 1995; Weickmann et al. 1997).

Before examining the temporal and spatial properties of the anomalous global friction and mountain torques, we examine the extent to which the angular momentum budget is balanced at each latitude. Figure 2a shows both the observed AAM tendency (contours) and the predicted AAM tendency (shading) as determined from the sum of each of the terms on the right-hand side (rhs) of (2). The difference between these two quantities is indicated in Fig. 2b. As can be seen, the budget is reasonably well balanced at most latitudes, particularly in the Southern Hemisphere where the torques are largest

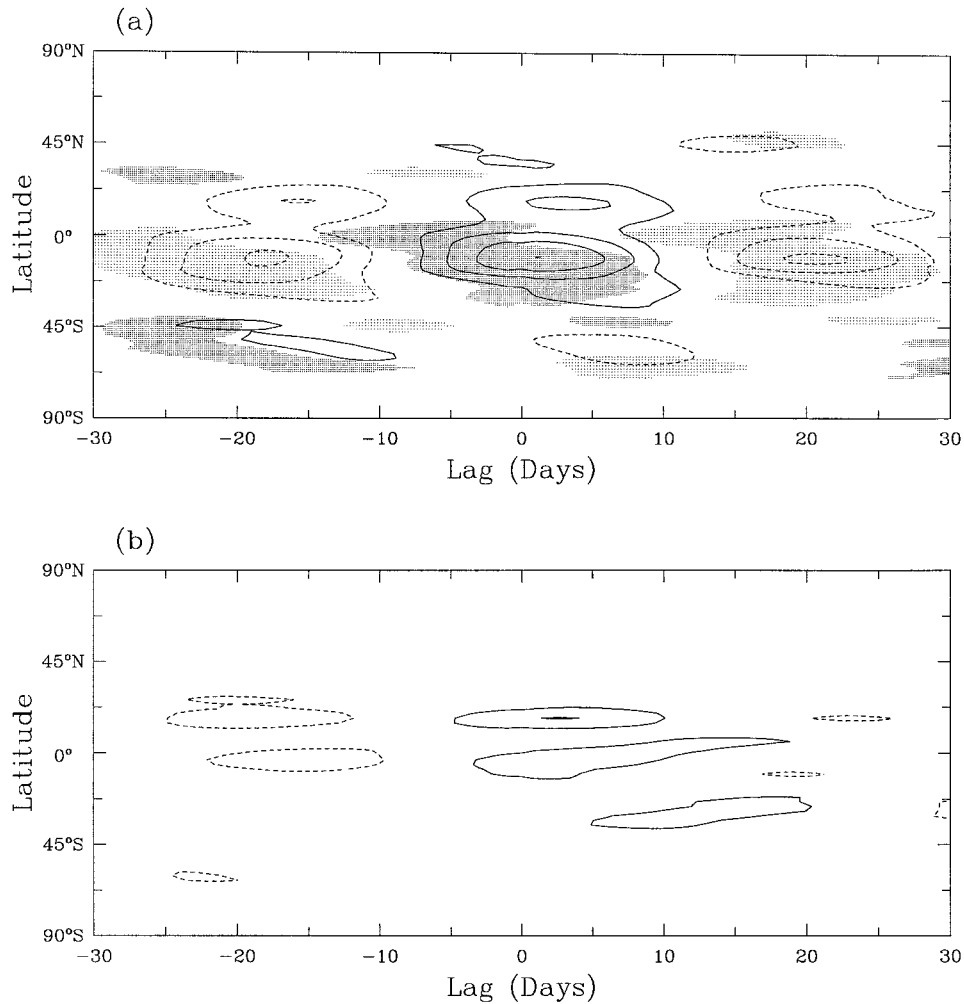


FIG. 2. (a) The observed anomalous AAM tendency (contours) and the predicted anomalous AAM tendency (shading) and (b) the difference between the observed and predicted AAM tendencies. The contour interval is $1.0 \times 10^{17} \text{ kg m}^2 \text{ s}^{-2}$. Shaded values exceed a magnitude of $1.0 \times 10^{17} \text{ kg m}^2 \text{ s}^{-2}$, with dark (light) shading denoting positive (negative) values.

(Fig. 3). Interestingly, the balance is weakest near the equator and in the Northern Hemisphere Tropics, the range of latitudes where the OLR anomalies is greatest (Fig. 6). A similar relationship between the latitude of the maximum OLR anomalies and the degree of angular momentum balance can also be seen in the boreal winter LOD–GAAM study of Weickmann et al. (1997, cf. their Fig. 9).

A decomposition of the two torques into functions of lag and latitude is shown in Fig. 3. Contours illustrate the value of the torque and stippling denotes values that exceed the 95% confidence level. It can be seen that the largest anomalous friction and mountain torques both occur within the subtropics and midlatitudes of the Southern Hemisphere. However, fairly substantial anomalous friction and mountain torques do extend into high latitudes. The most striking of these high-latitude

anomalous torques is the large mountain torque that reaches Antarctica at 80°S.

We next examine the particular geographical locations that are the dominant contributors toward the anomalous torques. This is performed for the friction torque by illustrating the anomalous $(\tau_\lambda)_{\sigma=1} \cos^2 \theta$ as a function of longitude and latitude at lag -6 (when the anomalous global friction torque is largest) and lag $+2$ days (see Fig. 4). As can be seen, the main contribution to the anomalous global friction torque comes from southeast Asia and Australia, and from the subtropical Indian and west Pacific Oceans.

We next address the question of whether it is the land or ocean contribution that dominates the anomalous global friction torque. The motivation for this question, as discussed in the introduction, arises from the observation of the large contemporaneous correlation be-

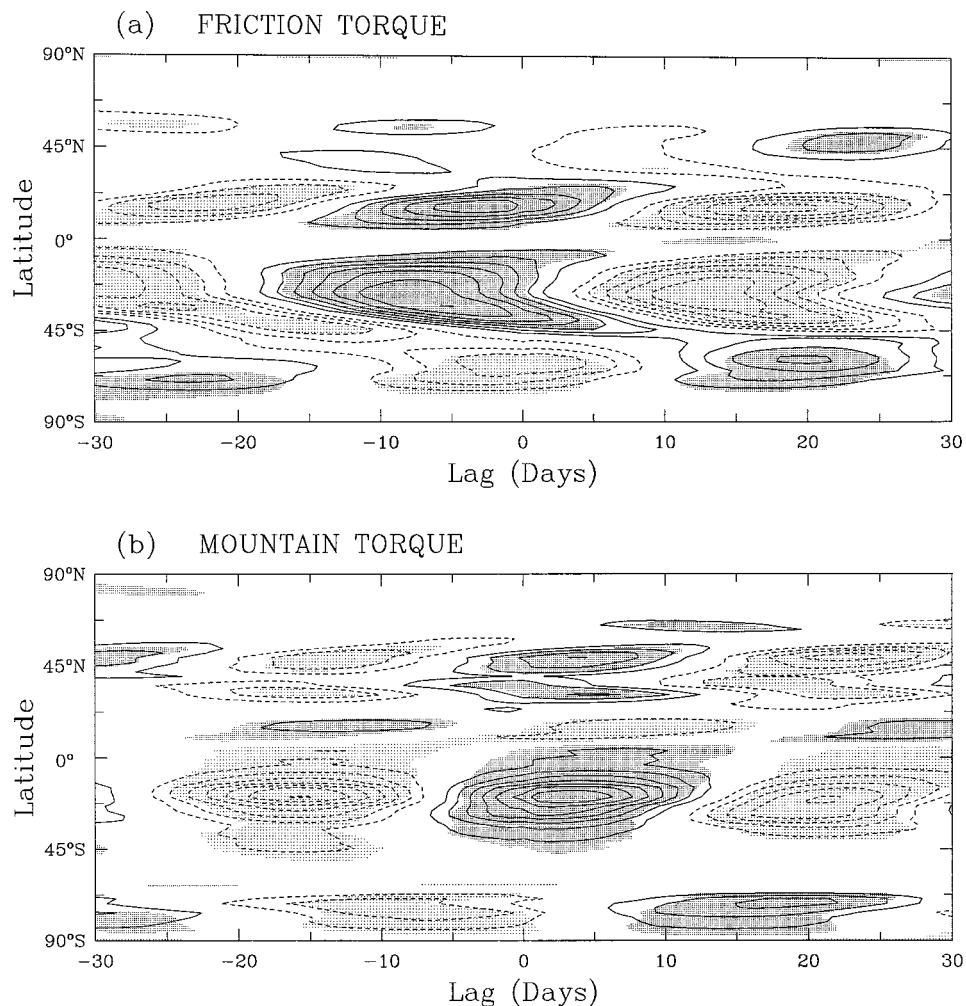


FIG. 3. (a) The anomalous zonal mean friction torque and (b) the anomalous zonal mean mountain torque regressed against the LOD tendency. The contour interval is $3.0 \times 10^{17} \text{ kg m}^2 \text{ s}^{-2}$. Solid contours are positive, dashed contours negative, and the zero contour is omitted. Shaded values exceed the 95% confidence level, with dark (light) shading denoting positive (negative) t values.

tween the LOD and GAAM time series. This implies that if the oceanic friction torque is large, then most of the angular momentum exchanged between the atmosphere and ocean must be rapidly transferred to the solid earth [using a barotropic ocean model, Ponte (1990) proposes that this rapid angular momentum transfer can be accomplished by barotropic Kelvin waves]. A calculation of the separate land and ocean contributions to the anomalous global friction torque does indeed verify that the ocean torque dominates at most lags. For example, at lag -6 days, the ratio of the ocean to land friction torque is found to be 3.1, and at lag $+2$ days this ratio equals 1.5.

The boreal winter LOD–GAAM study of Weickmann et al. (1997) also finds that the dominant anomalous surface stresses occur over water. However, compared with the present study, there are important differences

in the regions that are the primary contributors to the anomalous global friction torque. Although the tropical Pacific Ocean is important during both seasons, during the austral winter, the subtropical Indian Ocean also plays an important role, and during the boreal winter, it is the north Atlantic Ocean that also has a large anomalous friction torque. As there must be a rapid exchange of angular momentum between the ocean and solid earth during both seasons, these seasonal differences in the geographical locations of the ocean friction torque imply that there must be corresponding seasonal differences in the oceanic dynamical processes that account for this angular momentum exchange.

A similar analysis is performed for the anomalous mountain torque, shown as $p_s(\partial h/\partial x) \cos^2 \theta$ (Fig. 5). We first examine this quantity at lag $+4$ days, the time of the maximum anomalous global mountain torque (see

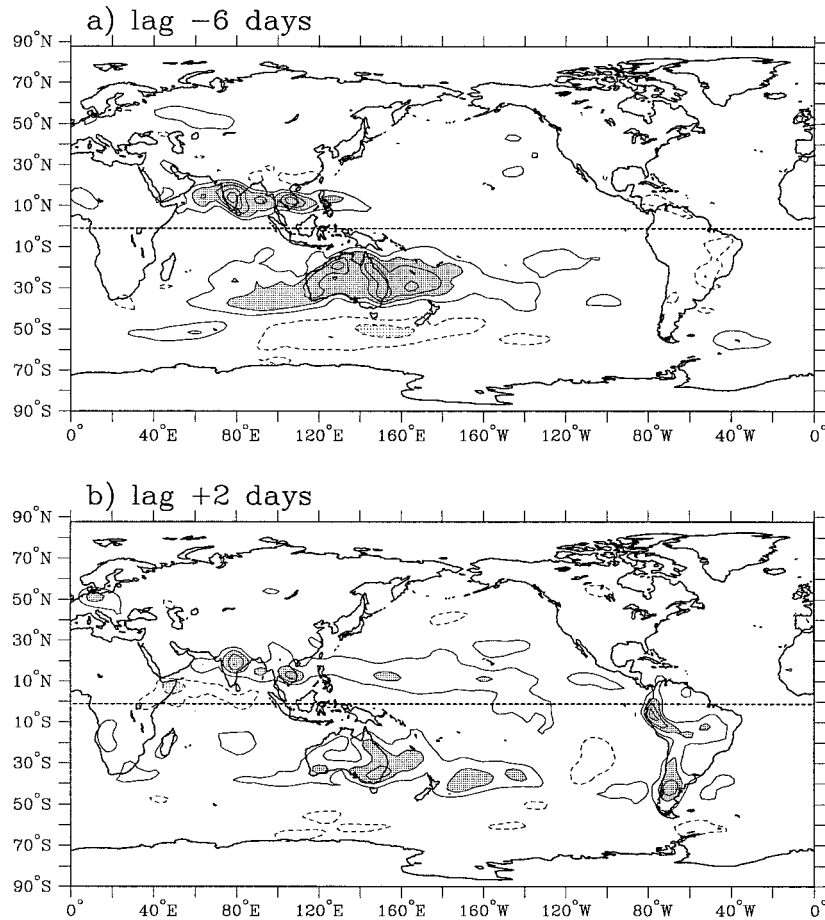


FIG. 4. The regression of the anomalous surface stress $(\tau_x)_{\sigma=1} \cos^2 \theta$ as a function of longitude and latitude at (a) lag -6 days and (b) lag $+2$ days. The contour interval is 0.003 N m^{-2} , and shaded values exceed a magnitude 0.006 N m^{-2} , with dark (light) stippling denoting positive (negative) values. Solid contours are positive, dashed contours negative, and the zero contour is omitted.

Fig. 5a). At this lag, it is obvious that the largest contribution to the anomalous global mountain torque comes from the Andes. The fractional contribution by particular mountain ranges toward the anomalous global mountain torque can be quantified by calculating the mountain torque due to particular regions. This calculation reveals that at lag $+4$ days, the fractional contribution by the Andes is 0.74 , and that from the Himalaya and Rockies is 0.25 and 0.01 , respectively. We also illustrate the anomalous $p_s(\partial h/\partial x) \cos^2 \theta$ at lag $+18$ days (Fig. 5b). At this lag, the anomalous Antarctic mountain torque reaches its largest value. Although the Antarctic mountain torque does not dominate the anomalous global mountain torque, it is nevertheless interesting that a torque of relatively large magnitude can exist so close to the earth's axis of rotation. As can be seen, the primary contribution from Antarctica is associated with Victoria Land, where there are high, steep mountains on the western boundary of the Ross Sea.

4. Dynamical processes associated with the torques

In this section, we first examine the OLR and eddy streamfunction fields, as anomalies of these quantities are closely linked to the generation of both friction and mountain torques. Next, we investigate the characteristics of the anomalous meridional circulation, in order to examine whether the anomalous friction torque is driven by fluctuations in the meridional circulation. This is followed by a calculation of the anomalous surface pressure field, in order to better understand the properties of the anomalous mountain torque.

a. Outgoing longwave radiation

Many studies have presented results that relate the anomalous friction and mountain torques associated with intraseasonal LOD–GAAM fluctuations to tropical convection. It has been suggested that the tropical convection can excite poleward-propagating Rossby waves

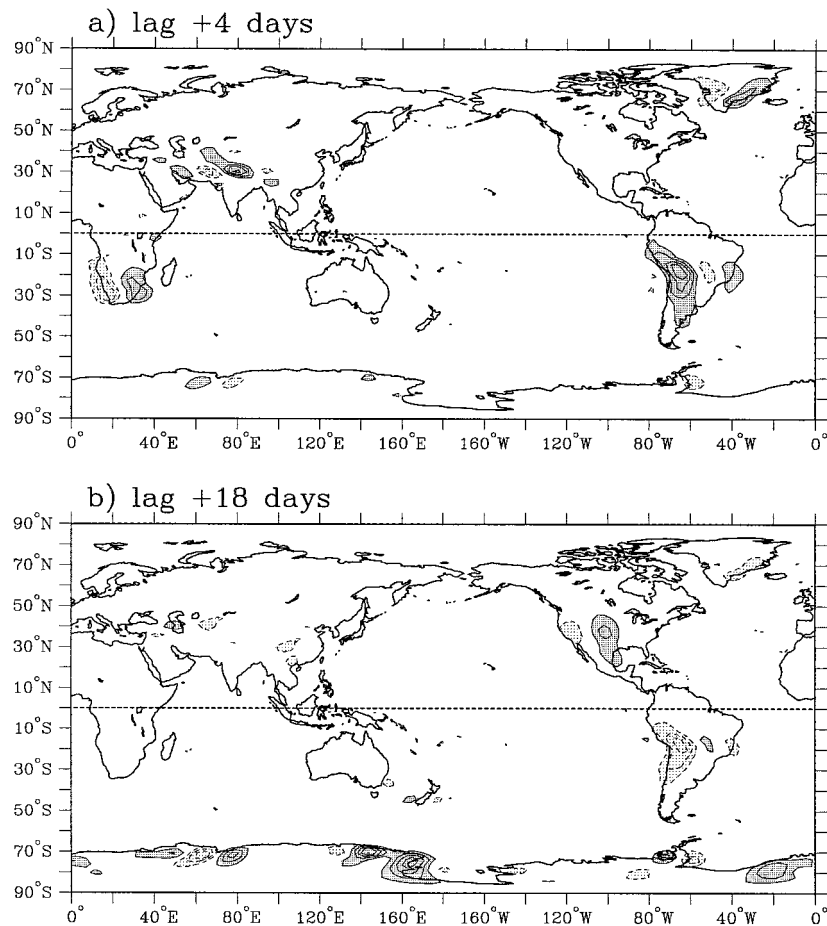


FIG. 5. The regression of the anomalous mountain torques, expressed as $p_s(\partial h/\partial x) \cos^2\theta$, as a function of longitude and latitude at (a) lag +4 days and (b) lag +18 days. The contour interval is 0.02 N m^{-2} , and shaded values exceed a magnitude 0.02 N m^{-2} , with dark (light) stippling denoting positive (negative) values. Solid contours are positive, dashed contours negative, and the zero contour is omitted.

whose surface eddy wind and pressure field can generate anomalous friction and mountain torques, respectively (Feldstein and Lee 1995). This process must involve the *eddy*, that is, deviation from zonal mean, component of the tropical convection. It has also been proposed that fluctuations in the zonal mean tropical convection can generate anomalous friction torques via fluctuations in the Coriolis torque acting on the low-level branch of the anomalous Hadley cell (Hendon 1995). For these reasons, in this section, we examine the detailed evolution of the OLR field, including its zonal mean.

The temporal evolution of the anomalous OLR field at specific lags is illustrated in Fig. 6 (note that a negative OLR anomaly implies enhanced convection). In order to emphasize its planetary-scale features, the OLR field is truncated to wavenumber three in the zonal direction. Calculations at less severe truncations, such as at zonal wavenumber six, yield essentially the same large-scale spatial patterns. As can be seen, at lag -8

days (Fig. 6a), which is two days before the anomalous global friction torque maximum, there is a large negative OLR anomaly confined primarily to the tropical Indian Ocean. Also, there are weak positive OLR anomalies over southeast Asia and the far northeastern tropical Pacific. At lag -3 days (Fig. 6b), the negative OLR anomaly in the Indian Ocean has further strengthened, expanded poleward in both hemispheres, and expanded eastward to cover the tropical northwestern Pacific. The positive OLR anomaly in the far northeastern tropical Pacific has also strengthened. At lag $+2$ days (Fig. 6c), which is two days prior to the anomalous global mountain torque maximum, the negative OLR anomaly in the Indian Ocean has slightly weakened and has moved farther northward into the Asian continent. At the same lag, the negative OLR anomaly in the west and central tropical Pacific has strengthened. At lag $+7$ days (Fig. 6d), the negative OLR anomaly over southern Asia has weakened, and a positive OLR anomaly has

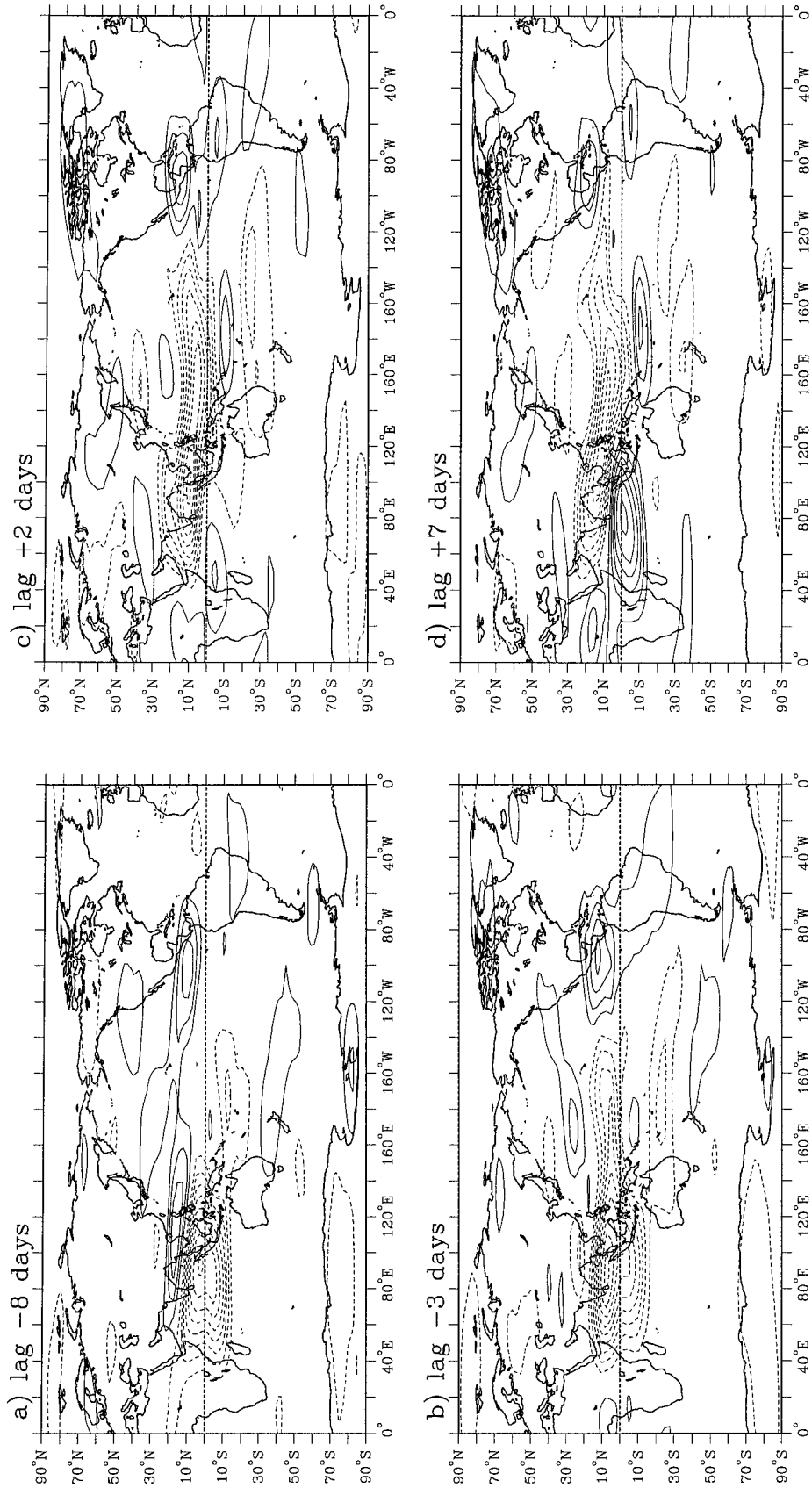


FIG. 6. The anomalous OLR regressed against the LOD tendency at (a) lag -8 days, (b) lag -3 days, (c) lag +2 days, and (d) lag +7 days. The contour interval is 0.6 W m^{-2} . Solid contours are positive, dashed contours negative, and the zero contour is omitted.

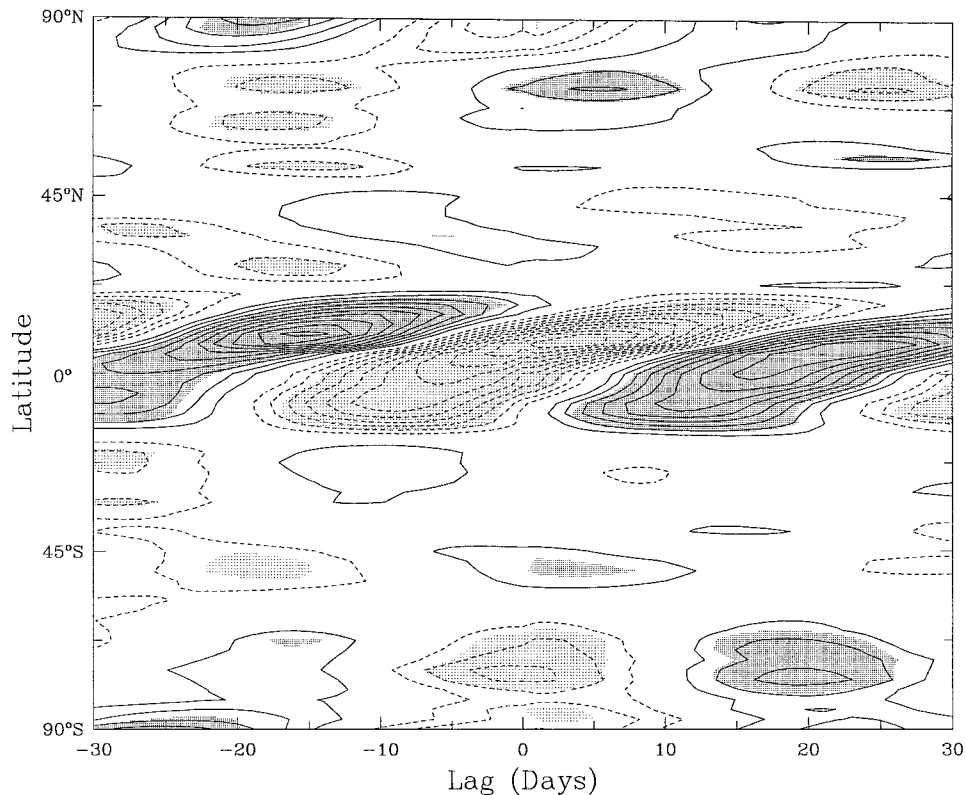


FIG. 7. The anomalous zonal mean OLR regressed against the LOD tendency. The contour interval is 0.15 W m^{-2} . Solid contours are positive, dashed contours negative, and the zero contour is omitted. Shaded values exceed the 95% confidence level, with dark (light) shading denoting positive (negative) t values.

formed over much of the equatorial Indian Ocean. This pattern for the OLR field is very similar to that at lag -13 days (not shown), but of opposite sign.

Two notable features in the above description of the OLR temporal evolution are also found in studies that examine the seasonal variation of the MJO. These are the northward propagation of an OLR anomaly from the equatorial Indian Ocean into the Asian continent during the austral winter, and the eastward OLR anomaly propagation from the Indian to the west Pacific Ocean that takes place throughout the year (e.g., Madden 1986; Knutson and Weickmann 1987; Wang and Rui 1990). Such northward OLR anomaly propagation has been associated with the active and break periods of the Asian summer monsoon (e.g., Yasunari 1980; Sikka and Gadgil 1980; Murakami 1984).

We next examine the anomalous zonal mean OLR as a function of lag and latitude (see Fig. 7). The most striking feature of the anomalous zonal mean OLR is its northward propagation. For example, proceeding from lag -10 days to lag $+10$ days, the extremes of the negative zonal mean OLR anomaly has shifted from about 10°S to 15°N . An examination of Fig. 6 reveals that much of this northward movement can be attributed to the northward movement of the negative OLR anomaly from the Indian Ocean into southeast Asia. Also,

Fig. 7 indicates that the convection is not simply a strengthening and weakening of a single sign anomaly, but at most stages during the LOD evolution, the anomalous zonal mean OLR takes on a dipole structure in the latitudinal direction.

b. Eddy streamfunction

In this section, we examine the anomalous 200-mb eddy streamfunction field and its relationship to the OLR field. In later sections, we will investigate the relationship between the anomalous 200-mb eddy streamfunction field and the anomalous friction and mountain torques. To the extent that there is a consistent relationship between the eddy streamfunction field and each of these quantities, we can hypothesize that the anomalous eddy streamfunction field provides the connection between the anomalous tropical convection and the anomalous friction and mountain torques.

One prominent feature in the temporal evolution of the eddy streamfunction field (see Fig. 8) is an eastward-propagating zonal wavenumber-one disturbance in the Tropics. In general, this disturbance consists of one pair of anticyclonic anomalies and another pair of cyclonic anomalies, both pairs straddling either side of the equator, with the anticyclonic (cyclonic) anomalies being

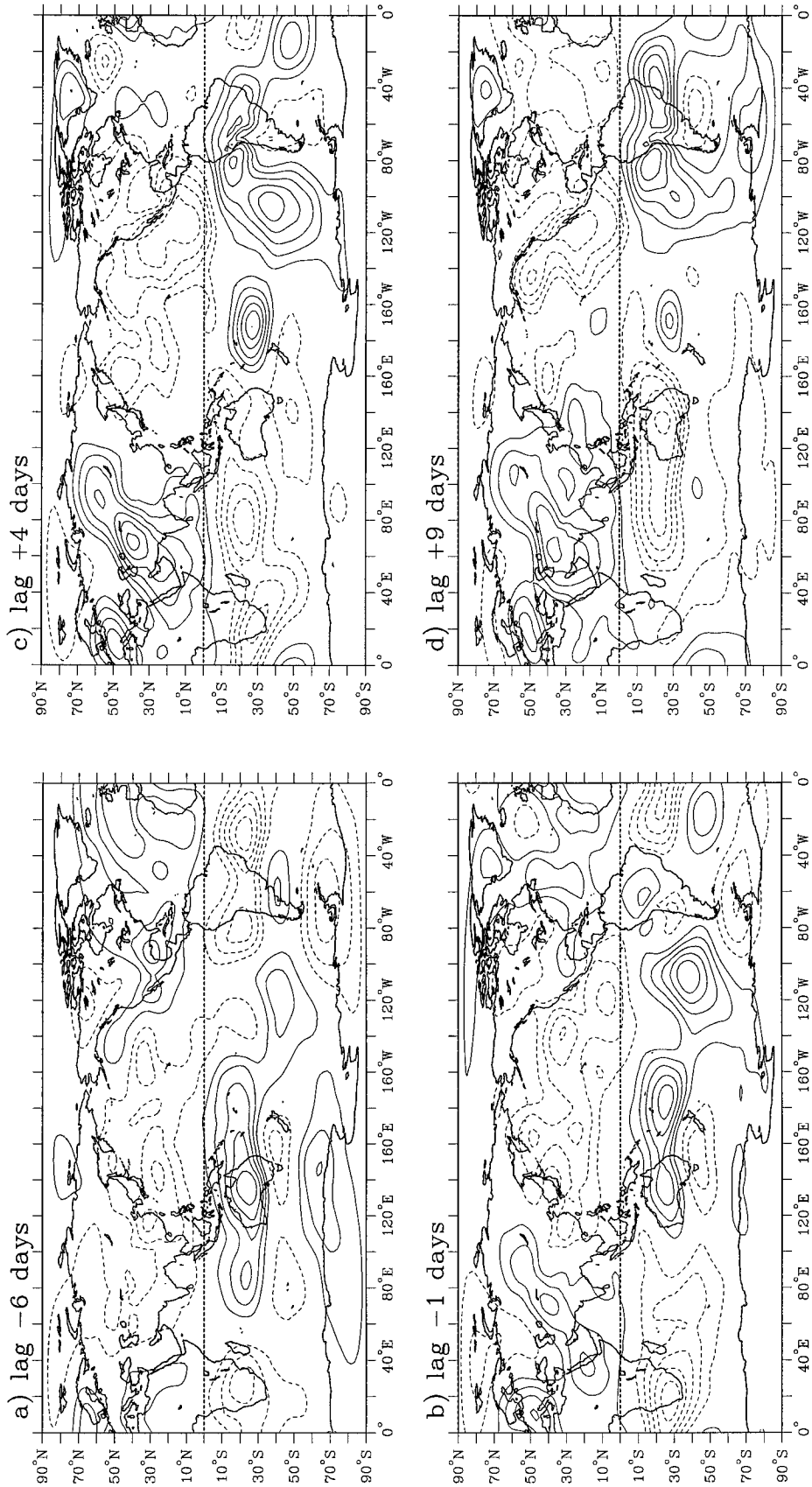


FIG. 8. The anomalous 200-mb eddy streamfunction regressed against the LOD tendency at (a) lag -6 days, (b) lag -1 days, (c) lag +4 days, and (d) lag +9 days. The contour interval is $4.0 \times 10^5 \text{ m}^2 \text{ s}^{-1}$. Solid contours are positive, dashed contours negative, and the zero contour is omitted.

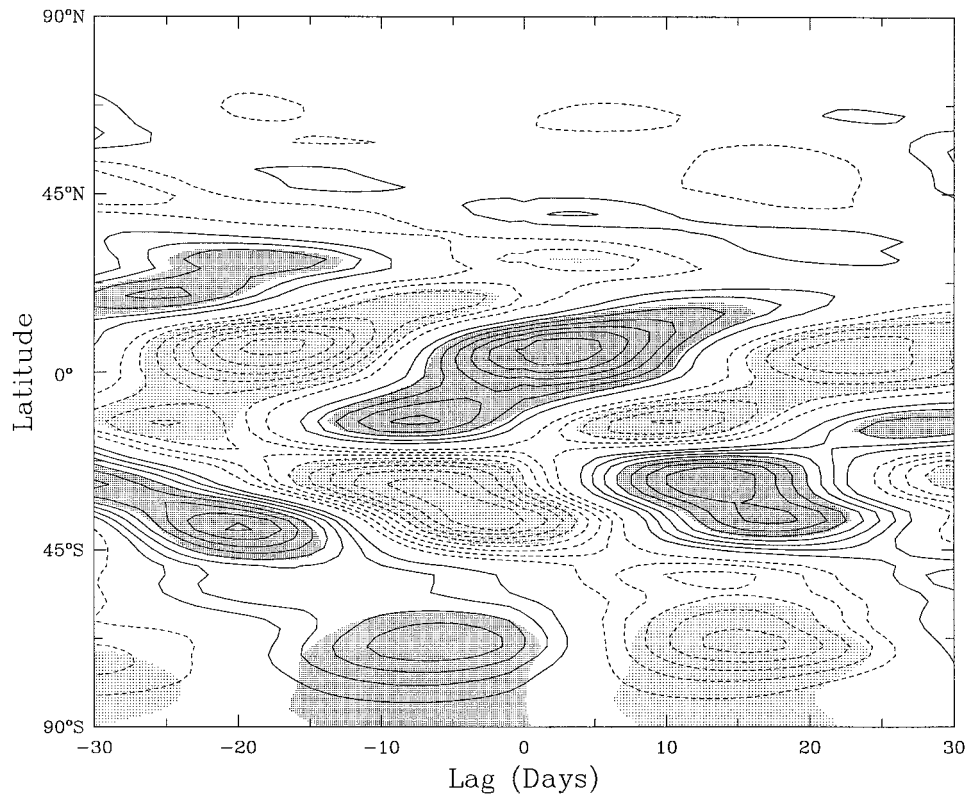


FIG. 9. The anomalous eddy AAM flux convergence regressed against the LOD tendency. The contour interval is $1.5 \times 10^{17} \text{ kg m}^2 \text{ s}^{-2}$. Solid contours are positive, dashed contours negative, and the zero contour is omitted. Shaded values exceed the 95% confidence level, with dark (light) shading denoting positive (negative) t values.

positioned west (east) of the maximum negative OLR anomaly. Furthermore, the location of these anomalies does bear some resemblance to what is found in steady-state primitive equation models that are forced by tropical diabatic heating anomalies (e.g., Ting and Sardeshmukh 1993). This same spatial relationship between the relative location of OLR, anticyclonic, and cyclonic anomalies is found for the MJO (e.g., Knutson and Weickmann 1987), providing further support for a close link between the MJO and intraseasonal LOD variability during the austral winter.

The anomalous eddy streamfunction field can also be related to the anomalous eddy AAM flux convergence (see Fig. 9). This relationship is important for better understanding the LOD fluctuations, since, as we will see in the next section, the amplitude and structure of the anomalous friction torque is closely linked to that of the anomalous eddy AAM flux convergence, via the meridional circulation. Before examining these relationships, it is helpful to first break up the anomalous eddy AAM flux into several contributing terms and write it as the vertical integral of the sum of linear, $[\bar{u}^*(p_s v)'] + [u'*(\bar{p}_s v)']$, and nonlinear, $[u'*(p_s v)']$, terms (see Weickmann et al. 1997), where an overbar (prime) denotes a time mean (deviation from the time mean). The

linear terms arise from the interaction between the transient eddy field, such as that displayed in Fig. 8, and the climatological eddy field, and the nonlinear terms result from the interactions among transient eddies. A calculation of the vertical integral of the meridional convergence of these terms finds that the linear terms contribute approximately 50% equatorward of 30° latitude in both hemispheres. Thus, if we were to assume that the anomalous wind field is primarily rotational, at the time of the largest anomalous linear eddy AAM flux convergence, the anomalous eddy streamfunction field should be near quadrature with the climatological eddy streamfunction field, as this longitudinal phase relationship maximizes the anomalous linear eddy AAM flux. A comparison of the location of the eddy streamfunction field in Fig. 8 with the upper-tropospheric climatological eddy streamfunction field (cf. James 1994, p. 167) does indeed reveal this relationship (not shown). Thus, the location of the anomalous eddy streamfunction field does contribute in an important manner to the strength of the anomalous eddy AAM flux, and hence, as we will see, to that of the anomalous friction torque.

Using scaling arguments, it is straightforward to show that the meridional convergence of the linear eddy AAM flux terms is proportional to $k(l^2 + 2lL + L^2)$, where

$k(l)$ is the zonal (meridional) wavenumber of the disturbance, and L the dominant meridional wavenumber of the austral winter climatological mean flow. Since zonal wavenumber one dominates the climatological upper-tropospheric eddy streamfunction within the Tropics during the austral winter (cf. James 1994, p. 167), disturbances with zonal wavenumber one and a large meridional wavenumber, such as the eddies shown in Fig. 8, have the preferred spatial structure for generating a large linear eddy AAM flux convergence.

c. Meridional circulations

In this section, we examine the role of anomalous meridional circulations in generating anomalous friction torques. In addition to the mechanism involving zonal mean tropical convection (Hendon 1995), as discussed at the beginning of section 4a, it has also been suggested that eddy-driven anomalous meridional circulations can alter the friction torque via the Coriolis torque acting on the anomalous low-level mean meridional winds (Weickmann and Sardeshmukh 1994; Weickmann et al. 1997). This process is simply an adjustment of the circulation toward thermal wind balance by the anomalous mean meridional circulation in response to the anomalous eddy momentum and heat fluxes. [For a review of the equations for the response of the meridional circulation to mechanical and thermal forcing, and driving by the eddy momentum and heat fluxes, see chapter 3 of Andrews et al. (1987).]

If anomalous meridional circulations play an important role during large LOD fluctuations, then the anomalous Coriolis and friction torques must be of similar magnitude at the lowest sigma level in the reanalysis model. We show this by examining the relative angular momentum equation, which can be written as

$$\begin{aligned} \frac{\partial}{\partial t}[p_s \mu_r] &= -\frac{1}{a \cos \theta} \frac{\partial}{\partial \theta} ([p_s \mu_r v] \cos \theta) - p_s f[v] a \cos \theta \\ &\quad - \frac{\partial}{\partial \sigma} \left([p_s \mu_r \dot{\sigma}] + g a \cos \theta [\tau_\lambda] + (a \cos \theta) \left[\sigma p_s \frac{\partial \phi}{\partial x} \right] \right), \end{aligned} \quad (7)$$

where τ_λ is the viscous stress, $\mu_r = ua \cos \theta$, f is the Coriolis parameter, and ϕ is the geopotential height. A calculation of each term in (7) at the reanalysis model's lowest sigma level finds that the zonal mean Coriolis torque [the second term on the rhs of (7)] is typically at least one order of magnitude larger than each of the other terms on both sides of (7), except for the friction torque term [the friction torque term in (7) is not calculated, because the internal viscous stresses are not readily available in the NCEP-NCAR reanalysis dataset]. This indeed verifies that the primary balance is

between the anomalous Coriolis and friction torques at the lowest model level. As an additional measure of the relationship between the Coriolis and friction torques, the linear pattern correlation between the lowest-level anomalous Coriolis torque and the anomalous surface friction torque is calculated and then averaged for each lag between ± 30 days [note that the surface friction torque, expressed in (3), differs from the lowest level friction torque in (7), since it does not involve a vertical derivative]. The resulting mean pattern correlation has a value of -0.91 . To some extent, this large correlation is not surprising, because the lowest-level friction torque is expected to be approximately proportional to the surface torque, since the viscous stresses decrease very rapidly with height.

The above relationship between the anomalous Coriolis and friction torques can be seen by examining the anomalous mass streamfunction [note that positive (negative) mass streamfunction contours correspond to a clockwise (counterclockwise) circulation in the meridional plane] (see Figs. 3a, 10). Inference of the anomalous Coriolis torque from the anomalous mass streamfunction shows that at each lag these two torques have a very similar spatial structure with opposite sign.

We next use this balance between the anomalous friction and Coriolis torques to address the question whether the friction torque is due to eddy surface wind anomalies, as described at the beginning of section 4a, or is generated by the anomalous meridional circulation. In order to examine this question, we separate the anomalous zonal mean surface stress into its zonal mean and eddy contributions. As the NCEP-NCAR reanalysis data uses a bulk parameterization scheme for the surface stress, that is, $(\tau_\lambda)_{\sigma=1} = -C_D u |V|$, where C_D is the surface drag coefficient, $|V|$ is the magnitude of the surface wind, and u is the surface zonal wind, one can write the anomalous zonal mean surface stress as

$$\begin{aligned} [(\tau_\lambda)_{\sigma=1}]' &= -[(C_D |\bar{V}|) * (u') *] - [(C_D |V'|) * (\bar{u}) *] \\ &\quad - [C_D |\bar{V}|][u'] - [C_D |V'|][\bar{u}]. \end{aligned} \quad (8)$$

This representation for the zonal mean surface stress neglects the temporally nonlinear terms, which were found to be negligible. The first and second terms on the rhs of (8) can be interpreted as representing the interaction between the anomalous surface eddy wind field and the climatological surface eddy wind field. If these terms were to dominate, it would imply that the anomalous meridional circulation and the associated Coriolis torque are primarily driven by the anomalous friction torque. In this case, the adjustment to thermal wind balance by the anomalous meridional circulation is driven by the change in the vertical wind shear due to the anomalous friction torque. The third and fourth terms on the rhs of (8) involve the anomalous zonal mean surface wind field. These terms are primarily due to the thermal wind adjustment as a result of the anomalous eddy heat and momentum flux forcing, as de-

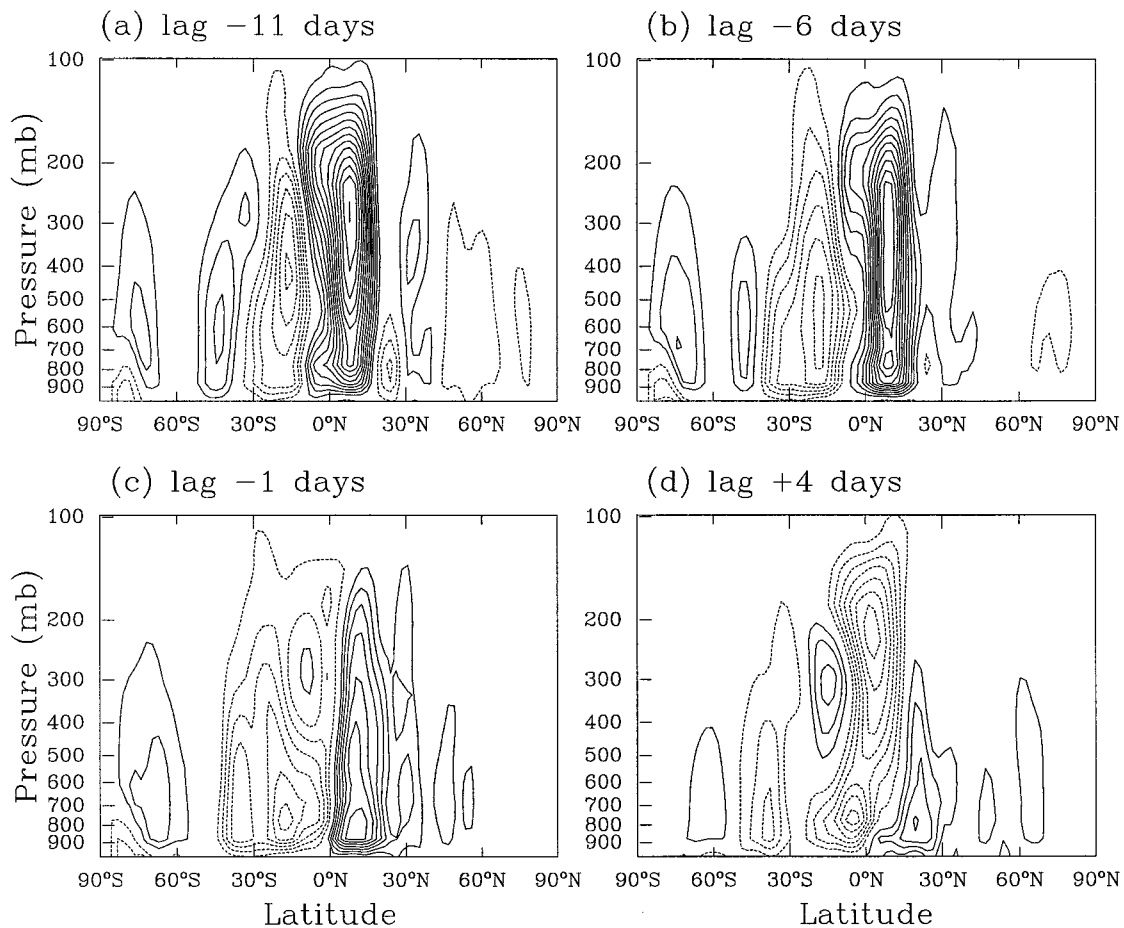


FIG. 10. The anomalous mass streamfunction regressed against the LOD tendency at (a) lag -11 days, (b) lag -6 days, (c) lag -1 days, and (d) lag $+4$ days. The contour interval is $5.0 \times 10^8 \text{ kg s}^{-1}$. Solid contours are positive, dashed contours negative, and the zero contour is omitted.

scribed earlier in this section. Thus, the dominance of these terms implies that the anomalous friction torque is driven by the anomalous Coriolis torque.

As the surface winds and drag coefficient are not readily available quantities in the NCEP–NCAR reanalysis dataset, it is not possible to precisely determine the value of each term on the rhs of (8). Instead, the approach we adopt is to estimate the surface wind with the NCEP–NCAR reanalysis wind field at the lowest model sigma level, and to estimate the surface drag coefficient following the procedure in Weickmann et al. (1997), where C_D is assigned a constant value of 1.5×10^{-3} over water and 6.5×10^{-3} over land. A comparison of this estimate of the anomalous friction torque (see Fig. 11c) with that shown in Fig. 3a indicates that these are reasonable approximations.

The zonal mean and eddy wind contributions to the anomalous friction torque are shown in Figs. 11a and 11b. It can be seen that the zonal mean contribution accounts for the vast majority of the Southern Hemisphere friction torque. On the other hand, in the Northern Hemisphere, the extremes of the zonal mean con-

tribution to the anomalous friction torque are typically about twice that of the eddy contribution. These results reveal that it is indeed the anomalous meridional circulation that is the primary contributor toward the driving of the anomalous friction torque.

There still remains the important question of whether it is the anomalous eddy fluxes or zonal mean heating that drive the anomalous meridional circulation. The answer to this question requires the solution of an inhomogeneous elliptic partial differential equation for the mass streamfunction, in which the forcing term is a function of the zonal mean heating and eddy fluxes. This question will be fully addressed in a separate paper. Nevertheless, there are hints from Fig. 9, which shows the anomalous eddy AAM flux convergence, that this quantity is indeed important for driving the anomalous meridional circulation.

If the anomalous eddy AAM flux is an important factor in driving the anomalous meridional circulation, one expects that 1) the latitude at the center of the anomalous mass streamfunction cells should approximately coincide with that of the anomalous eddy AAM flux

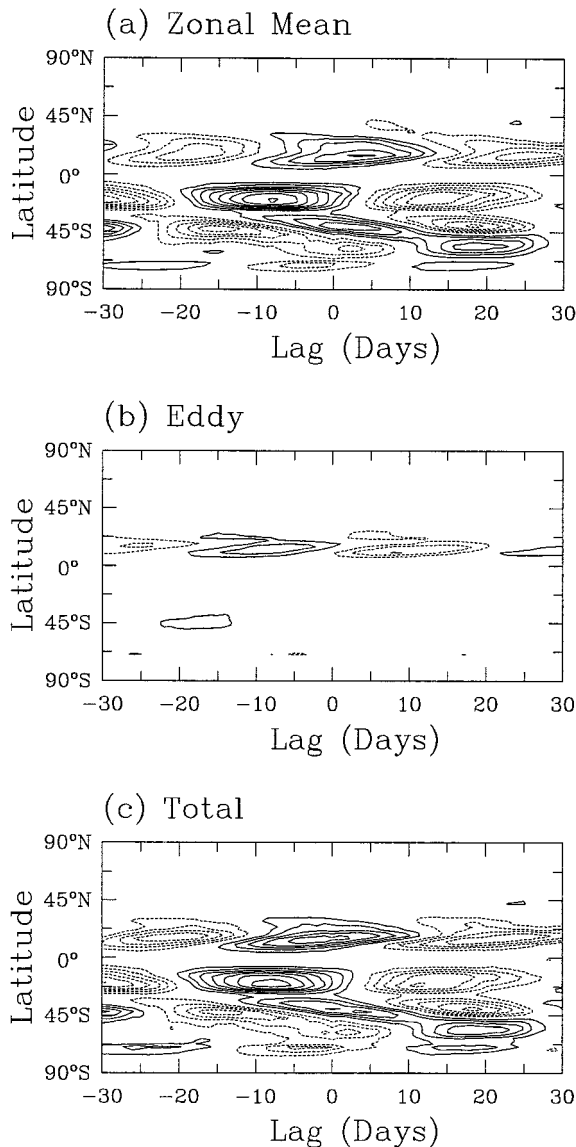


FIG. 11. The contribution to the anomalous zonal mean friction torque from its (a) zonal mean wind component, (b) eddy component, and (c) the sum of (a) and (b). The contour interval is $3.0 \times 10^{17} \text{ kg m}^2 \text{ s}^{-2}$. Solid contours are positive, dashed contours negative, and the zero contour is omitted. See the text for details describing how these quantities are approximated.

convergence and 2) the anomalous low-level Coriolis torque must be of the same sign as the anomalous eddy AAM flux convergence. This is because it is found that the anomalous eddy AAM flux convergence is confined to the upper troposphere, and an adjustment to thermal wind balance by the anomalous meridional circulation would require the above characteristics. Upon examining the anomalous eddy AAM flux convergence, one can see that at lag -6 days, there are regions of negative anomalous eddy AAM flux-convergence between 15° and 45°S and poleward of about 5°N . Furthermore, there is a positive anomalous eddy AAM flux convergence

between 15°S and 5°N . The corresponding anomalous meridional circulations that would lead to a thermal wind adjustment are two thermally direct anomalous cells, one between 5° and 35°N , the other between 15° and 45°S , and two thermally indirect anomalous cells, straddling either side of the equator between 15°S and 5°N . Comparison with Fig. 10b reveals a very good match outside of the deep Tropics. Within the deep Tropics, where the vertical extent of the meridional circulation is shallow due to the small Rossby depth scale, the match is reasonably good in the Southern Hemisphere and poor in the Northern Hemisphere. However, given the fact that the anomalous friction torque is negligible inside the deep Tropics (Fig. 3a), these results suggest that the driving of the anomalous friction torque by the eddy AAM fluxes is indeed an important process. With regard to the anomalous eddy heat flux (not shown), large values are found only in the Southern Hemisphere, centered at 45°S . Such eddy heat fluxes will drive anomalous meridional circulations at the same latitude. However, as large anomalous friction torques are not found at this latitude, it is likely that the anomalous eddy heat flux does not play an important role in the LOD variability.

One can get an appreciation of the role of the zonal mean heating by comparing Figs. 7 and 10. As expected, the latitude of the negative OLR extremes closely coincides with that of the maximum anomalous vertical winds as inferred from the anomalous mass streamfunction. This relationship is apparent between lag -11 and lag $+4$ days as both the negative OLR extrema and the center of the two tropical cells move northward together. Furthermore, because the above eddy flux analysis suggests that the eddies do not directly drive the entire anomalous deep tropical meridional circulation, it is likely that at least the low-latitude anomalous meridional circulation is in part driven by the anomalous zonal mean heating. However, because the present analysis cannot distinguish whether or not the zonal mean heating is itself driven by the eddies, it is not possible to speculate whether a zonal mean heating anomaly, independent of the eddy driving, plays an important role in driving the anomalous friction torque.

d. Eddy surface pressure

In order to investigate the relationship between the anomalous eddy streamfunction field and the anomalous mountain torque, it is useful to examine the anomalous eddy surface pressure field. This is illustrated in Fig. 12 at lag $+4$ days, the time of the maximum anomalous global mountain torque. It can be seen that the anomalous mountain torque at South America is associated with a surface anticyclone on the eastern side of the Andes that extends over a large fraction of the continent. The anomalous mountain torque at the Himalaya is associated with a weak surface cyclone on the western side of the mountains.

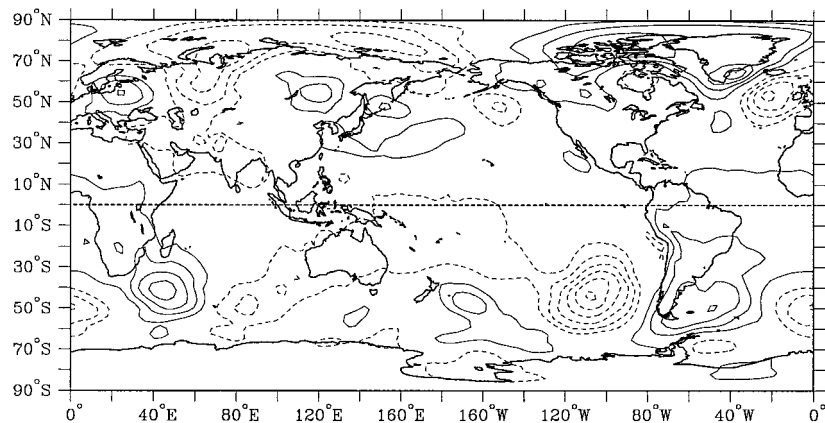


FIG. 12. The anomalous surface pressure regressed against the LOD tendency at lag +4 days. The contour interval is 20.0 N m^{-2} . Solid contours are positive, dashed contours negative, and the zero contour is omitted.

A comparison between the anomalous eddy streamfunction and eddy surface pressure fields at lag +4 days reveals a complex relationship between these two fields (see Figs. 8c, 12). However, in general, the eddy surface pressure anomalies tend to occur in similar geographical locations as the eddy streamfunction anomalies. An examination of the signs of the anomalies of both fields suggests a baroclinic structure in the Tropics, and an equivalent barotropic structure in middle and high latitudes. For example, east of the Andes, the 200-mb eddy streamfunction field consists of a relatively strong (weak) upper-tropospheric anticyclone (cyclone) that overlaps with the southern (northern) half of the surface anticyclone. This indicates that the Andean mountain torque is associated with a disturbance of both baroclinic and barotropic characteristics. In the Himalaya region, where most of the mountain torque occurs at a lower latitude than in the Andes, the eddy surface pressure and streamfunction anomalies have opposite sign, revealing that this particular mountain torque is linked to a baroclinic disturbance.

These results imply that one cannot simply infer the sign of the anomalous mountain torque by assuming that the anomalous surface pressure field resembles the anomalous upper-tropospheric streamfunction. Presumably an understanding of these properties can be obtained with the aid of potential vorticity inversions (Hoskins et al. 1985).

5. Conclusions

The primary aims of this study are both to document the spatial and temporal properties of the friction and mountain torques and to investigate several of the basic atmospheric dynamical processes associated with intraseasonal LOD variability during the austral winter. For this purpose, we use the LOD timeseries, the NCEP-NCAR reanalysis dataset, and OLR, and regress a number of different quantities against the LOD tendency.

It is found that the anomalous global friction torque leads the anomalous global mountain torque by about eight days. The largest contributions to the anomalous global friction torque occur at Australia and the adjacent Indian and Pacific Oceans, and southeast Asia, while the largest anomalous mountain torque is mostly due to the Andes. A closer examination of the anomalous friction torque reveals that the dominant contribution comes from ocean surfaces, implying that ocean dynamics must rapidly transfer angular momentum to the solid earth during the austral winter.

The regression analysis yielded results that suggest that the friction and mountain torques are both driven by the response of the atmospheric circulation to the diabatic heating field associated with the MJO. This response to the MJO heating includes an anomalous meridional circulation, which excites the anomalous global friction torque via an anomalous Coriolis torque, and a direct eddy response to the diabatic heating, which has the appropriate phase relative to the topography to generate a large mountain torque. Although this analysis did suggest that the anomalous meridional circulation is forced by the anomalous eddy AAM fluxes, and that the anomalous eddy AAM fluxes were in turn driven by the MJO heating, the analysis also points to possible forcing of the anomalous meridional circulation by zonal mean heating, as suggested by Hendon (1995).

The results of this study raise several important questions on intraseasonal LOD variability. However, these questions are not limited to the austral winter, as they are equally relevant for the boreal winter. For example, both the present investigation and the intraseasonal boreal winter LOD-GAAM study of Weickmann et al. (1997) find relationships to tropical convection. To place this relationship on firmer grounds, it would be necessary to use either a barotropic or a multilevel baroclinic model and examine the response to diabatic heating anomalies resembling those found in observations. Furthermore, the link between the anomalous upper-

tropospheric eddy streamfunction field and anomalous eddy surface pressure field, and hence the anomalous mountain torque, is found to be rather complex. Last, there remains the question of whether the anomalous friction torque is driven by the zonal mean eddy angular momentum flux or the zonal mean diabatic heating. This question is also particularly relevant for the boreal winter, as the analysis of section 4c as applied to the boreal winter also reveals that the anomalous friction torque is driven by the anomalous meridional circulation. The latter of these three questions is a subject of ongoing research.

Acknowledgments. This research was supported by the National Aeronautics and Space Administration through Grant NAG5-6207. I would like to thank Drs. Sukeyoung Lee, Richard Rosen, Klaus Weickmann, and three anonymous reviewers for their beneficial comments. I would also like to thank the NOAA Climate Diagnostics Center for providing me with the NCEP-NCAR reanalysis dataset, and Dr. Peter Nelson of the Atmospheric and Environmental Research, Inc., for providing me with the LOD time series.

REFERENCES

- Anderson, J. D., and R. D. Rosen, 1983: The latitude-height structure of 40–50 day variations in atmospheric angular momentum. *J. Atmos. Sci.*, **40**, 1584–1591.
- Andrews, D. G., J. R. Holton, and C. B. Leovy, 1987: *Middle Atmosphere Dynamics*. Academic Press, 489 pp.
- Davis, R., 1976: Predictability of sea surface temperature and sea level pressure anomaly over the North Pacific Ocean. *J. Phys. Oceanogr.*, **6**, 249–266.
- Dickey, J. O., M. Ghil, and S. L. Marcus, 1991: Extratropical aspects of the 40–50 day oscillation in length-of-day and atmospheric angular momentum. *J. Geophys. Res.*, **96**, 22 643–22 658.
- Feldstein, S. B., 1998: An observational study of the intraseasonal poleward propagation of zonal mean flow anomalies. *J. Atmos. Sci.*, **55**, 2516–2529.
- , and S. Lee, 1995: The intraseasonal evolution of angular momentum in aquaplanet and realistic GCMs. *J. Atmos. Sci.*, **52**, 625–649.
- Hendon, H. H., 1995: Length of day changes associated with the Madden-Julian oscillation. *J. Atmos. Sci.*, **52**, 2373–2383.
- Hide, R., and J. O. Dickey, 1991: Earth's variable rotation. *Science*, **253**, 629–637.
- , N. T. Birch, L. V. Morrison, D. J. Shea, and A. A. White, 1980: Atmospheric angular momentum fluctuations and changes in the length of day. *Nature*, **286**, 114–117.
- Hoskins, B. J., M. E. McIntyre, and A. W. Robertson, 1985: On the use and significance of isentropic potential vorticity maps. *Quart. J. Roy. Meteor. Soc.*, **111**, 877–946.
- Itoh, H., 1994: Variations of atmospheric angular momentum associated with intraseasonal oscillations forced by zonally varying prescribed heating. *J. Geophys. Res.*, **99**, 12 981–12 998.
- James, I. N., 1994: *Introduction to Circulating Atmospheres*. Cambridge University Press, 422 pp.
- Kang, I.-S., and K.-M. Lau, 1990: Evolution of tropical circulation anomalies associated with 30–60 day oscillation of globally averaged angular momentum during northern summer. *J. Meteor. Soc. Japan*, **68**, 237–249.
- Knutson, T. T., and K. M. Weickmann, 1987: 30–60 day atmospheric oscillations: Composite life cycles of convection and circulation anomalies. *Mon. Wea. Rev.*, **115**, 1407–1436.
- Langley, R. B., R. W. King, I. I. Shapiro, R. D. Rosen, and D. A. Salstein, 1981: Atmospheric angular momentum and length of day: A common fluctuation with a period near 50 days. *Nature*, **294**, 730–732.
- Lau, K.-M., I.-S. Kang, and P.-J. Sheu, 1989: Principal modes of intraseasonal variations in atmospheric angular momentum and tropical convection. *J. Geophys. Res.*, **94**, 6319–6332.
- Madden, R. A., 1986: Seasonal variations of the 40–50 day oscillation in the Tropics. *J. Atmos. Sci.*, **43**, 3138–3158.
- , and P. Julian, 1971: Detection of a 40–50 day oscillation in the zonal wind. *J. Atmos. Sci.*, **28**, 702–708.
- , and —, 1972: Description of global-scale circulation cells in the Tropics with a 40–50 day period. *J. Atmos. Sci.*, **29**, 1109–1123.
- , and P. Speth, 1995: Estimates of atmospheric angular momentum, friction, and mountain torques during 1987–88. *J. Atmos. Sci.*, **52**, 3681–3694.
- Magana, V., 1993: The 40- and 50-day oscillations in atmospheric angular momentum at various latitudes. *J. Geophys. Res.*, **98**, 10 441–10 450.
- Murakami, M., 1984: Analysis of the deep convective activity over the western Pacific and southeast Asia. Part II: Seasonal and intraseasonal variations during the northern summer. *J. Meteor. Soc. Japan*, **62**, 88–108.
- Peixoto, J. P., and A. H. Oort, 1992: *Physics of Climate*. American Institute of Physics, 520 pp.
- Ponte, R. M., 1990: Barotropic dynamics and the exchange of angular momentum between the oceans and solid earth. *J. Geophys. Res.*, **95**, 11 369–11 374.
- , and R. D. Rosen, 1993: Determining torques over the ocean and their role in the planetary momentum budget. *J. Geophys. Res.*, **98**, 7317–7325.
- Rosen, R. D., 1993: The axial momentum balance of earth and its fluid envelope. *Surv. Geophys.*, **14**, 1–29.
- , and D. A. Salstein, 1983: Variations in atmospheric angular momentum on global and regional scales and length of day. *J. Geophys. Res.*, **88**, 5451–5470.
- Sikka, D. R., and S. Gadgil, 1980: On the maximum cloud zone and the ITCZ over Indian longitudes during the southwest monsoon. *Mon. Wea. Rev.*, **108**, 1840–1853.
- Ting, M., and P. D. Sardeshmukh, 1993: Factors determining the extratropical response to equatorial diabatic heating anomalies. *J. Atmos. Sci.*, **50**, 907–918.
- Wang, B., and H. Rui, 1990: Synoptic climatology of transient tropical intraseasonal convection anomalies: 1975–1985, 1990. *Meteor. Atmos. Phys.*, **44**, 43–61.
- Weickmann, K. M., and P. D. Sardeshmukh, 1994: The atmospheric angular momentum cycle associated with a Madden-Julian oscillation. *J. Atmos. Sci.*, **51**, 3194–3208.
- , S. J. S. Khalsa, and J. Eischeid, 1992: The atmospheric angular-momentum cycle during the tropical Madden-Julian oscillation. *Mon. Wea. Rev.*, **120**, 2252–2263.
- , G. N. Kiladis, and P. D. Sardeshmukh, 1997: The dynamics of intraseasonal atmospheric angular momentum oscillations. *J. Atmos. Sci.*, **54**, 1445–1461.
- Yasunari, T., 1980: A quasi-stationary appearance of 30 to 40 day period in the cloudiness fluctuations during the summer monsoon over India. *J. Meteor. Soc. Japan*, **58**, 225–229.